INTERNATIONAL ATOMIC ENERGY AGENCY
UNITED NATIONS EDUCATIONAL, SCIENTIFIC AND CULTURAL ORGANIZATION

INTERNATIONAL CENTRE FOR THEORETICAL PHYSICS
34100 TRIESTE (ITALY) - P.O.B. 586 - MIRAMARE - STRADA COSTIERA 11 - TELEPHONE: 2240-1
CABLE: CENTRATOM - TELEX 460393 - I

SMR/208 - 10

SPRING COLLEGE IN MATERIALS SCIENCE

ON

"METALLIC MATERIALS"

(11 May - 19 June 1987)

INTRODUCTION TO LIQUID METAL ALLOYS

M.P. TOSI
Dipartimento di Fisica Teorica
Università di Trieste
Trieste
Italy

I INTRODUCTION TO LIQUID METAL ALLOYS

M. P. Tosi

Dipartimento di Fisica Teorica, Università di Trieste, Italy

1. Phase diagrams

In order to introduce a preliminary classification of different types of liquid binary alloys[1], we remind the reader in Fig. 1 of the various types of phase diagrams that these systems may exhibit.

Diagram (a) is for the Ag-Au system, whose components have the same valence and closely similar atomic volumes (see Table 1). This is clearly the simplest type of phase diagram, showing a complete range of solutions in both the solid and the liquid. Diagram (b) is instead for Cu-Zn: although this alloy of heterovalent elements shows a variety of solid phases, with characteristic crystal structures which become stable over limited ranges of concentration (b.c.c. β-brass, complex-cubic γ-brass and h.c.p. ε-brass, the various ranges of stability being essentially governed by the electron/atom ratio $c_1Z_1 + c_2Z_2$ in a manner first described by Hume-Rothery), we do not need to draw a sharp distinction between this type of system and a system with a phase diagram of type (a) if we are concerned only with their liquid phase.

Table 1. Valence Z and molar volume V of the elements whose phase diagrams are discussed in the text

Element	Au	Ag	Cu	Zn	Pb	Al	Sb
Z	1	1	1	2	4	3	5
V (cc)	11.5	11.6	7.95	9.95	12.5	8.7	7.9

Diagrams (c) and (d) refer instead to Ag-Cu and to Pb-Zn. The Ag-Cu system shows a characteristic eutectic behaviour: the two constituents are only slightly soluble in one another in the solid, which therefore tends to separate into a Ag-rich phase and a Cu-rich phase, but they become completely miscible in the liquid. Low solubility at low temperature implies that the internal energy of mixing ΔE is positive (and of the order of a few tenths of an eV per atom if the solubility is down to a few percent at a temperature of several hundred centigrades): this energy falls on melting (to a value of order 0.05 eV per atom in the middle of the composition range for Cu-Ag), so that the mutual solubility is greater

[1] T. E. Faber, "Theory of Liquid Metals" (Cambridge University Press, 1972).

in the liquid phase. In the Pb-Zn system the internal energy of mixing in the solid is still positive but so large that the solubility of Pb in Zn cannot be shown on the scale of the diagram (and the solubility of Zn in Pb is just barely visible): in spite of the decrease of ΔE on melting, there is still partial miscibility in the liquid phase till the temperature is raised sufficiently, above a critical temperature (which is about 800C for Pb-Zn).

For the systems discussed up to this point, the different phase behaviours are in qualitative correlation with differences in size and in valence of the constituents, as a quick look to Table 1 will show. All these systems should be contrasted with the Al-Sb system, whose phase diagram is shown in (e). The new feature here is the appearance of the compound AlSb in the solid phase, which is particularly stable (energy of mixing of order -0.5 eV per atom at concentration c = 0.5, and high melting temperature). It is clear that chemical bonding (and not purely valences and sizes) is now playing a role. To emphasize this point, we show in (f) the phase diagram of the Cs - I system, which at c = 0.5 forms the ionic compound cesium iodide.

We shall immediately below sharpen up the distinction between "normal" metallic alloys and compound-forming binary liquids by contrasting their observed liquid structure. We shall then proceed with the discussion of "normal" alloys, with the exclusion of compound-forming systems. Progress can be made in understanding the former systems by adaptation and extension of the concepts already developed for pure liquid metals. Compound-forming systems will be taken up separately later.

2. Liquid structure of binary liquids

In a binary liquid, three pair distribution functions are evidently required for a complete description of liquid pair structure. Denoting by $4\pi r^2 n_\beta g_{\alpha\beta}(r)dr$ the average number of β-type atoms in a spherical shell centred on an α-type atom (where a Greek suffix labels the atomic species and $n_\alpha = c_\alpha n_i$ is the number of atoms of species α per unit volume in the alloy), and introducing the corresponding partial structure factors $a_{\alpha\beta}(k)$ by

$$a_{\alpha\beta}(k) = 1 + 4\pi n_i \int_0^\infty [g_{\alpha\beta}(r) - 1] \frac{\sin(kr)}{kr} r^2 \, dr$$

the coherently scattered X-ray (or neutron) intensity I(k) is given by

$$I(k) \propto n_1 f_1^2 + n_2 f_2^2 + \frac{n_1^2}{n_i} f_1^2 [a_{11}(k) - 1] + \frac{n_2^2}{n_i} f_2^2 [a_{22}(k) - 1]$$
$$+ \frac{2 n_1 n_2}{n_i} f_1 f_2 [a_{12}(k) - 1] \qquad \left(k = \frac{4\pi}{\lambda} \sin\theta\right)$$

the f's being the scattering amplitudes of the two atomic species. We have used above, the definitions and notation given by Faber and Ziman[1] for the partial structure factors. An alternative definition, given by Ashcroft and Langreth[2], is

$$S_{\alpha\beta}(k) = \delta_{\alpha\beta} + 4\pi\sqrt{n_\alpha n_\beta}\int_0^\infty [g_{\alpha\beta}(r) - 1]\frac{\sin(kr)}{kr} r^2\, dr$$

leading to

$$I(k) \propto f_1^2\, S_{11}(k) + f_2^2\, S_{22}(k) + 2 f_1 f_2\, S_{12}(k) \qquad \left(k = \frac{4\pi}{\lambda}\sin\theta\right)$$

Complete resolution of the three partial diffraction patterns in the above expressions for the scattered intensity is allowed by multi-pattern neutron diffraction methods based on isotopic enrichment: these involve neutron scattering from three samples of the same chemical material prepared with different isotopic concentrations, these sample having the same partial structure factors (in the classical limit) but different isotope-averaged scattering amplitudes. The partial structure factors measured by this method[3] in the liquid Cu-Sn system at composition Cu_6Sn_5 are shown in Fig. 2. These clearly show resemblance with the partial structure factors of a mixture of hard spheres which are shown in Fig. 3 (at equimolar composition in the Percus-Yevick approximation). Thus, gross features of the short range order in "normal" liquid alloys are (as in pure liquid metals) associated with screened-ion sizes.

The data in Figure 2 for the liquid Cu-Sn system near equimolar composition should be contrasted with those of an ionic material such as NaCl in the liquid state[4], which are shown in Figure 4. The obvious differences are that $S_{NaNa}(k)$ and $S_{ClCl}(k)$ are closely similar (in particular, their main peaks are in phase) and that $S_{NaCl}(k)$ has developed a deep valley. On Fourier transform one sees that these features imply chemical short-range order i.e. a first neighbour shell around any given ion which is composed of ions of the other species (see Figure 5). Similar qualitative features characterize the liquid structure of compound-forming metallic alloys such as Li-Pb at the "stoichiometric" concentration Li_4Pb,[5] whereas no such type of order is seen in the pair distribution functions of Cu_6Sn_5.

The most direct way to emphasise the degree of chemical short range order in the primary diffraction data is to construct from them the so-called Bhatia-Thornton structure factors[6], expressing the correlations between fluctuations

[2] N. W. Ashcroft and D. C. Langreth, Phys. Rev. **156**, 685 (1967).
[3] J. E. Enderby, D. M. North and P. A. Egelstaff, Phil. Mag. **14**, 961 (1966).
[4] F. G. Edwards, J. E. Enderby, R. A. Howe and D. I. Page, J. Phys. C **8**, 3483 (1975); S. Biggin and J. E. Enderby, J. Phys. C **15**, L305 (1982).
[5] H. Ruppersberg and H. Reiter, J. Phys. F **12**, 1311 (1982).
[6] A. B. Bhatia and D. E. Thornton, Phys. Rev. B **2**, 3004 (1970).

variables which are the fluctuation N(r) in the total particle density (irrespectively of the species) and the fluctuation in concentration c(r). These variables are defined by

$$N(r) = n_1(r) + n_2(r) \quad \text{and} \quad c(r) = \frac{n_2}{n_1} n_1(r) - \frac{n_1}{n_1} n_2(r)$$

and the corresponding structure factors are

$$S_{NN}(k) = c_1 S_{11}(k) + c_2 S_{22}(k) + 2\sqrt{c_1 c_2}\, S_{12}(k)$$
$$S_{cc}(k) = c_1 c_2\left[c_2 S_{11}(k) + c_1 S_{22}(k) - 2\sqrt{c_1 c_2}\, S_{12}(k)\right]$$
$$S_{Nc}(k) = c_1 c_2\left[S_{11}(k) - S_{22}(k) + (c_2 - c_1) S_{12}(k) / \sqrt{c_1 c_2}\right]$$

These are shown in Figure 6 for the Cu_6Sn_5 liquid alloy, from the experimental data of Figure 2. It is seen that $S_{NN}(k)$ is very similar to the standard structure factor of a pure liquid metal, whereas $S_{cc}(k)$ lacks any significant structure, being at all values of k very close to the value c_1c_2 that it would have in an ideal random alloy. The Bhatia-Thornton structure factors $S_{NN}(k)$ and $S_{cc}(k)$ for molten NaCl, shown in Figure 7, show instead that the most remarkable structural features in this liquid are associated with $S_{cc}(k)$ i.e. with chemical short range order. Finally, we show in Figure 8 the concentration-concentration structure factor $S_{cc}(k)$ of liquid Li_4Pb as measured by neutron diffraction[5].

3. Thermodynamic properties and solution models for "normal" liquid binary alloys

In discussing pure liquid metals we have seen that the long-wavelength limit $S(k \to 0)$ of their structure factor is directly related to the mean square fluctuation $\langle(\Delta N)^2\rangle$ of the number of particles in a given volume and hence to the isothermal compressibility. Similar relations hold for a binary alloy[7], whose liquid structure factors are determined at long wavelengths by the isothermal compressibility, the concentration dependence of the molar volume, and the mean square fluctuation $\langle(\Delta c)^2\rangle$ in the composition of the alloy. In particular,

$$S_{cc}(0) = N\langle(\Delta c)^2\rangle = N k_B T \Big/ \left(\frac{\partial^2 G}{\partial c^2}\right)_{T,P} = (1-c) \Big/ \left(\frac{\partial \log a}{\partial c}\right)_{T,P} \qquad (3.1)$$

where c is the solute concentration, G is the Gibbs free energy of the alloy and a is the activity of the solute, related to its chemical potential by $\mu - \mu_0 = k_B T \log a$.[8] This difference in chemical potentials (relative to the pure state of the solute) can be measured as an electromotive force in a suitable electromotive cell, an example of such data being shown in

[7] J. G. Kirkwood and F. Buff, J. Chem. Phys. **19**, 774 (1951).
[8] L. S. Darken, Trans. Metall. Soc. AIME **239**, 80 (1967).

Figure 9 for the liquid Na-Cs alloy.[9] We note immediately that concentration fluctuations of long wavelength will be enhanced (relative to a random alloy) in systems which show a tendency to phase separation (phase diagrams of types (c) or (d) in Figure 1) and depressed near the "stoichiometric" composition in compound-forming systems. Indeed, they are totally supressed by charge neutrality in a molten salt.

The Gibbs free energy G can be written

$$G = N\left[c_1 G_1^{(0)} + c_2 G_2^{(0)}\right] + G_m$$

which defines the Gibbs free energy of mixing G_m, $G_\alpha^{(0)}$ being the Gibbs free energies per atom of the pure components at the same pressure and temperature as the alloy. Clearly, the data shown in Figure 9 allows direct test of solution models for G_m.

The simplest realistic model of concentration fluctuations in "normal" liquid alloys seems to be the conformal solution model of Longuet-Higgins[10] or the regular solution model in the zeroth order approximation[11]. The free energy of mixing is written

$$G_m = Nk_BT\left[c \log c + (1-c) \log (1-c)\right] + Nc(1-c)w \qquad (3.2)$$

The first term arises from the ideal entropy of mixing: thus, if $w=0$ one gets an ideal random alloy (for which it is easily seen from eqn (3.1) that $S_{cc}(0) = c(1-c)$). The quantity w is an "interchange energy", assumed in these models to be independent of concentration, such that if a nearest-neighbour A-A pair and a similar B-B pair are replaced by two A-B pairs, the energy of the alloy increases by $2w/z$, z being the number of nearest neighbours of an atom. A positive w implies that like-atom nearest neighbour pairs are energetically preferred over unlike-atom pairs, and therefore (if w is large) a tendency towards phase separation. In effect, the validity of the model requires two conditions[12]:

(i) The size difference between the two types of atoms is not too large, roughly $1/2 < v_1^{(0)}/v_2^{(0)} < 2$ where the vs are the atomic volumes of the two pure species;

(ii) w/z should be small compared with the thermal energy k_BT, since otherwise the random distribution of atoms utilized in obtaining the expression (3.2) for G_m is not appropriate. A more detailed analysis suggests $|w/k_BT| < 2$ as an appropriate range of approximate validity of the model.

Using eqn (3.2), with w independent of concentration, in eqn (3.1) one finds

[9] K. Ichikawa and J. C. Thompson, J. Phys. F **4**, 9 (1974).
[10] H. C. Longuet-Higgins, Proc. Roy. Soc. A **205**, 247 (1951).
[11] See e.g. E. A. Guggenheim, "Mixtures" (Oxford University Press, 1952).
[12] A. B. Bhatia, in "Liquid Metals" (Inst. of Phys. Conf. Series No. 30, Bristol 1976).

$$S_{cc}(0) = \frac{c(1-c)}{1 - c(1-c)(2w/k_BT)}$$

Good agreement with the experimental data for Na-K liquid alloys has been found for $w = 1.1 k_BT$.[13] This has allowed in turn an evaluation of the liquidus curve for this system,[14] with results which are shown in Figure 10. The same model is expected to hold also for other alloys, for example Ag-Au and Cd-Zn, for which the above conditions are met. However, even when these conditions are satisfied, G_m can have considerable asymmetry about $c = 1/2$ in some alloys, for example Cd-Pb. One would need to introduce a concentration dependence in the interchange energy to account for such asymmetry.

Flory[15] has argued that when the ratio $b = v_1^{(0)}/v_2^{(0)}$ of the atomic volume is appreciably different from unity, eqn (3.2) is more appropriately replaced by

$$G_m = Nk_BT\left[c \log \phi + (1-c) \log (1-\phi)\right] + Nw\phi\left[c + (1-c)/b\right]$$

where $\phi = cb/[1-c+cb]$ is the concentration by volume. The above expression has been found by Bhatia and March[16] to reproduce the main features of experimental data for the Na-Cs alloy system. A direct comparison with the measured electromotive force is shown in Figure 9, and Figure 11 reports a similar comparison for the liquidus curve. It may be noted that the eutectic concentration $c_{Na} \approx 0.2$ in this system corresponds to a very large peak in $S_{cc}(0)$ versus concentration, denoting a strong enhancement of concentration fluctuations at this composition.

3.1 Electron theory of heat of mixing and interchange energy. The semiempirical theory given by Miedema and coworkers[17] for the heat of mixing $\Delta H_m(c)$ in an A_cB_{1-c} metallic alloy identifies major electronic factors in the difference $n_A - n_B$ in the electron densities at the boundary of bulk atomic cells of the A and B metal and in the difference $\phi_A - \phi_B$ in the metallic electronegativities. Their expression for the heat of mixing is

$$\Delta H_m(c) = c(1-c^s)\,\Delta H_s(A \text{ in } B)$$

$$c^s = c\, v_A^{(0)2/3}\left[c\, v_A^{(0)2/3} + (1-c)\, v_B^{(0)2/3}\right]^{-1}$$

$$\Delta H_s(A \text{ in } B) = 2\, v_A^{(0)2/3}\left[n_A^{-1/3} + n_B^{-1/3}\right]^{-1}\left[-P(\Delta\phi)^2 + Q(\Delta n^{1/3})^2\right]$$

[13] A. B. Bhatia, W. H. Hargrove and N. H. March, J. Phys. C **6**, 621 (1973).
[14] A. B. Bhatia and N. H. March, Phys. Lett. **41 A**, 397 (1972).
[15] P. J. Flory, J. Chem. Phys. **10**, 51 (1942).
[16] A. B. Bhatia and N. H. March, J. Phys. F **5**, 1100 (1975).
[17] A. R. Miedema, F. R. deBoer and P. F. de Chatel, J. Phys. F **3**, 1558 (1973); A. R. Miedema, P. F. de Chatel and F. R. de Boer, Physica **100 B**, 1 (1980).

where c^s is the cell surface concentration of the A species, P and Q are positive constants, and Δ denotes the difference between the two components. This expression yields a successful classification of a very great number of alloys, with both positive and negative heats of mixing (see Figure 12).

Comparing the above expression with the conformal solution form, Alonso and March[18] extracted a concentration-dependent interchange energy w(c) as

$$w(c) = \frac{v_B^{(0)2/3}}{c\,v_A^{(0)2/3} + (1-c)\,v_B^{(0)2/3}}\,\Delta H_s(\text{A in B})$$

This yields in particular

$$w(0)/w(1) = \left[v_A^{(0)}/v_B^{(0)}\right]^{2/3} = \frac{\Delta H_s(\text{A in B})}{\Delta H_s(\text{B in A})}$$

The data shown in Table 2 suggest a dependence of the interchange energy on concentration in several liquid alkali metal alloys, where the above ratio is appreciably different from unity.

Table 2. Test of conformal solution theory for liquid alkali metal alloys

Alloy (AB)	NaCs	NaRb	NaK	KCs	RbCs	KRb
$[v_A^{(0)}/v_B^{(0)}]^{2/3}$	0.48	0.57	0.64	0.76	0.82	0.88
ΔH_s(A in B) / ΔH_s(B in A)	0.28	0.49	0.62	0.44	1.0	1.0

4. Electrical resistivity and electromigration in normal alloys

4.1 Electric resistivity. It is generally observed that the electric resistivity of a binary liquid alloy is a smooth function of concentration at constant temperature. Figure 13, taken from the book of Faber[1], reports some examples of observed behaviours.

A basis for qualitative understanding of these data is provided by the Faber-Ziman theory,[19] which extends to alloys the weak scattering Ziman approach for pure liquid metals. The essential assumptions are the nearly-free-electron

[18] J. A. Alonso and N. H. March, Physica 114 B, 67 (1982).
[19] T. E. Faber and J. M. Ziman, Phil. Mag. 11, 153 (1965).

model for the conduction electrons and the idea that the scattering of electrons at the Fermi level by a single screened ion of species α may be represented by some self-consistent screened pseudopotential $V_\alpha(k)$, which is weak enough that the scattering process may be described by the first Born approximation. The resistivity ρ is conveniently written as the sum of two terms, $\rho = \rho' + \rho''$ with

$$\rho' = \langle [c_1 V_1^2(k) + c_2 V_2^2(k)]\, a(k) \rangle \,, \qquad \rho'' = \langle c_1 c_2 [V_1(k) - V_2(k)]^2 [1 - a(k)] \rangle$$

with

$$\langle f(k) \rangle = \frac{3\pi m^2 n_i}{\hbar^3 e^2 k_F^2} \int_0^1 f(k) \left(\frac{k}{2k_F}\right)^3 4d\left(\frac{k}{2k_F}\right)$$

$$a(k) = \frac{c_1^2 V_1^2(k) a_{11}(k) + 2c_1 c_2 V_1(k) V_2(k) a_{12}(k) + c_2^2 V_2^2(k) a_{22}(k)}{c_1^2 V_1^2(k) + 2c_1 c_2 V_1(k) V_2(k) + c_2^2 V_2^2(k)}$$

Clearly, a(k) is an effective-interaction-averaged structure factor, which for qualitative purposes may be visualized as similar to the structure factor of a pure liquid metal.

The concentration dependence enters these formulas in many ways (density and Fermi momentum, effective interactions, structure factors) but again for qualitative purposes, at least if the two components of the alloy are not greatly different in valences and sizes, we may assume that it is described by the explicit concentration factors in ρ' and ρ'': the former term then varies roughly linearly between the resistivities of the two pure liquid metals whereas the latter gives rise to a parabolic deviation. This deviation is expected to be (a) positive for an alloy of monovalent metals, where $2k_F$ lies well below the main peak in the structure factor, (b) negative for an alloy of divalent metals, where $2k_F$ lies just above the main peak in the structure factor, and (c) essentially negligible for an alloy of polyvalent metals, where $2k_F$ lies in the region where the structure factor is essentially unity (see Figure 14). This reasoning, which parallels the explanation given in the Ziman theory for the temperature dependence of the resistivity of pure liquid metals in dependence of their valence (a positive temperature coefficient of the resistivity in monovalent metals, a negative one for divalent metals and a small coefficient for polyvalent metals), leads to predicted resistivity isotherms which are shown in Figure 15, in qualitative accord with the observed behaviours shown in Figure 13 (convex resistivity isotherms for monovalent systems like Na-K and almost linear isotherms for polyvalent ones like Sn-Pb and Sb-Bi). A more complex argument is needed for alloys of heterovalent elements, where the variation of k_F with concentration has to be taken into account: resistivity isotherms of the type shown in Figure 13 for Cu-Sb appear as a possible behaviour.

A great deal of numerical calculations of the resistivity of liquid metallic alloys have been reported in the literature, a sample being shown in Figure 13 for the Na-K system. Special cases are the amalgams of Hg with other metals, where a large drop of resistivity is observed in alloying. A specific effect of concentration fluctuations on scattering of the

conduction electrons in systems with a miscibility gap has been observed as a decrease of resistivity in the neighbourhood of the critical point. Faber[1] argues that the enhancement of concentration fluctuations at long wavelengths subtracts from the structure factors, and hence from the scattering, in the region of relatively larger wave numbers which are most important in resistive scattering.

4.2 Electromigration. The constituents of an alloy tend to separate when a d.c. current is passed through it, the resulting steady state being one in which a gradient of concentration is set up and the current-induced drift is balanced by diffusion in the reverse direction. The drift velocity v_d acquired by the solute in a field E can be written within the limits of the Nernst-Einstein relation as

$$v_d = Z^* |e| E D / k_B T$$

where D is the diffusion coefficient of the solute: this equation defines the effective valence Z^* of the solute in the electromigration process. In the steady state we have for the concentration c(x) of the solute (the balance condition)

$$-D \frac{dc}{dx} = c v_d$$

and hence

$$c(x) \propto \exp\left[-\frac{v_d x}{D}\right] \propto \exp\left[-\frac{Z^* |e| E x}{k_B T}\right]$$

which allows the determination of Z^* from experiment. The experimental results suggest a connection between the sign of Z^* (i. e. the direction in which the solute migrates) and the sign of $-d\rho/dc$. For instance, in the Na + K system the Na migrates to the anode (i. e. $Z^*_{Na} < 0$) when c_{Na} is small but to the cathode when c_{Na} is large, the change in sign occurring near the concentration where the resistivity has a maximum (see Figure 13).

A connection between the electromigration process and the electrical resistivity can be seen by the following argument[1]. The effective force $Z^* |e| E$ that the solute experiences is the sum of the field force $Z |e| E$, Z being the true valence of the solute, and of the force F due to the electrons that collide with it (i. e. due to the current, which is not in general directly to the field):

$$Z^* |e| E = Z |e| E + F$$

On the other hand, since the electrons do not accelerate, the field force $-n|e|E$ on the electrons must be balanced by the total force $n_i F_T$ exerted by the system of screened ions in electron-ion collisions. With $F_T = -[(1-c) F_{solvent} + c F]$ one finds

$$(1-c) F_{solvent} + c F = -\frac{n_i}{n} |e| E = -Z_{av} |e| \rho j$$

where Z_{av} is the average valence of the alloy. A separation between $F_{solvent}$ and F is allowed by the Faber-Ziman theory of the resistivity, yielding

$$F = -Z_{av} |e| \frac{3\pi m^2 n_i}{\hbar^3 e^2 k_F^2 \rho} \langle V_2^{2(k)} + c V_2^2(k)[a_{22}(k) - 1] + (1-c) V_1(k) V_2(k)[a_{12}(k) - 1] \rangle E$$

Here, the suffixes 1 and 2 denote the solvent and the solute, respectively, and the angular brackets have the meaning already shown in § 4.1. For a dilute alloy the above expression can be simplified by further approximation to yield

$$Z^* \approx -\left[\frac{1}{2\rho}\left(\frac{d\rho}{dc}\right)\right]_{\text{pure solvent}}$$

in the case of a monovalent solvent, and

$$Z^* \approx Z_{solute} - \frac{\rho_{\text{pure solute}}}{\rho_{\text{pure solvent}}} Z_{solvent}$$

if both solvent and solute are polyvalent. These crude predictions describe the trend of the experimental results, as is seen in Table 3.

Table 3. Effective valence Z^* of solutes in electromigration[1]

Solute	K	Cd	Hg	Tl	Pb	Na	Hg	Tl	Pb	Ga	Bi
Solvent	Na	Na	Na	Na	Na	K	K	K	K	Sn	Sn
Temp. (C)	100	110	110	–	110	100	100	110	100	300	350
Z^*_{expt}	-0.8	-13	(-18)	(-18)	(-21)	-0.5	-10	-20	-22	+0.6	-0.8
Z^*_{theor}	-5	-28	30	–	-60	-4	-18	–	–	+0.8	-5.7

It was first shown by Haeffner[20] that isotopic separation occurs in a chemically pure liquid metal under passage of a large d.c. current density over long times. In all systems where the Haeffner effect has been observed, the lighter isotope collects at the anode. Faber[1] argues for a similarity with observations on solid metals, showing that a concentration gradient of lattice vacancies is set up under a strong current. Fluctuations from the average force exerted on the ion system by the electron collisions may tend to be above the average near light ions, which would then be preferentially dragged along by the current and collect at the anode.

5. Chemical short range order in liquid alloys

Fully ionized salts with a large band gap like the alkali halides remain ionic across melting. On the other hand, melting of covalent semiconductors such as Ge or InSb involves a collapse of the covalent structure, directly revealed by an increase of coordination from 4 to values in the range 6 - 8 and by an increase in electrical conductivity to an essentially metallic type. Between these extremes, a number of systems have been identified which show a variety of intermediate electronic behaviours in the liquid phase. With varying concentration away from stoichiometry, one can cross in the liquid state the border areas between the canonical types of bonding in solids (ionic systems, electronic semiconductors and metals, molecular systems).[21,22,23]

Among these liquid systems special attention has been given recently to (i) alloys of metallic elements having a relatively large difference in electronegativity, such as Cs - Au or Li - Pb and other alloys of alkalis with Pb and In, which form intermetallic compounds at certain stoichiometric compositions in the solid state; (ii) solutions of alkali metals and alkali halides; and (iii) alloys based on chalcogens such as Cu - Te or Ni - Te.

5.1 Cesium - gold alloys. The stoichiometric compound CsAu crystallizes in the CsCl-type structure and is a strongly polar semiconductor with an optical band gap of 2.6 eV at room temperature. Its electrical conductivity drops on melting to a value which is comparable to that of molten salts. Electromigration experiments on the melt give evidence that Cs migrates to the cathode and Au to the anode, one Cs^+ and one Au^- being transported per elementary charge to the electrodes.

[20] E. Haeffner, Nature **172**, 775 (1973).
[21] J. E. Enderby, in "The Metal - Nonmetal Transition in Disordered Systems" (ed. L. R. Friedman and D. P. Tunstall; The University of Edinburgh, 1979).
[22] F. Hensel, Adv. Phys. **28**, 555 (1979).
[23] M. Rovere and M. P. Tosi, Rept. Progr. Phys. **49**, 1001 (1986).

Measurements of electrical conductivity, magnetic susceptibility and nuclear magnetic resonance on the melt show that for small concentrations of excess cesium (excess concentration less than about 7%) the excess electrons are in localized states. We report in Figure 16 from Sotier et al[24] a comparison of the electrical conductivities of Cs - CsAu and Cs - CsX systems (where X = halogen) across the full range of composition. Very similar electronic behaviours are clearly indicated for all these systems, with some marginal differences near stoichiometry. At low concentration of excess metal, it is known for the alkali - alkali halide systems, from optical absorption and other experiments, that the excess electrons are trapped in states which are the liquid state analogues of F centres in the solid, with residence times of the order of 10^{-12} sec as estimated from nuclear relaxation rates[25]. Somewhat shorter residence times, of the order of 10^{-13} sec, are suggested for the localized excess electrons in Cs - CsAu near stoichiometry. A continuous transition from an essentially ionic to a metallic melt is seen in Figure 16 to occur as the concentration of the alkali is increased towards the pure liquid metal. The same transition is shown in Figure 17 through data on the excess magnetic susceptibility for several alkali - alkali halide systems[26]. The susceptibility is of paramagnetic type and becomes close to the Curie value for an isolated electron spin as stoichiometry is approached.

Neutron diffraction measurements[27] of the liquid structure of Cs - Au alloys over a range of composition up to 80% Cs show a rather strong degree of chemical short range order (Cs preferentially surrounded by Au in the first neighbour shell and vice versa): the Cs - Au first neighbour distance at 3.6 Å can be followed up to 80 % Cs and the Cs - Cs distance at 5.9 Å which is characteristic of the pure liquid Cs metal emerges at 70 % Cs, these distances being little sensitive to composition. Furthermore, well away from stoichiometry a rapid increase in the intensity scattered at small angles is observed, which indicates large density fluctuations at long wavelength becoming allowed by conduction electron screening.

5.2 Short range order and Mott transition in alkali - gold alloys. A connection between local chemical order in the liquid alloy and the opening of a pseudogap in the electron energy spectrum was demonstrated in a tight binding approach by Kittler and Falicov[28]. Franz et al[29] have developed the model up to detailed contact with the experimental evidence. They write a tight binding Hamiltonian

[24] S. Sotier, H. Ehm and F. Maidl, J. Non-Cryst. Solids **61/62**, 95 (1984).
[25] S. Sotier and W. W. Warren, J. Physique Coll. **41**, C8 - 40 (1980); R. Dupree, D. J. Kirby, W. Freyland and W. W. Warren, Phys. Rev. Lett. **45**, 130 (1980); W. W. Warren, S. Sotier and G. Brennert, Phys. Rev. Lett. **50**, 1505 (1983).
[26] N. Nicoloso and W. Freyland, Zs. Physik. Chem. **135**, 39 (1983).
[27] W. Martin, W. Freyland, P. Lamparter and S. Steeb, Phys. Chem. Liquids **10**, 61 (1979).
[28] R. C. Kittler and L. M. Falicov, J. Phys. C **9**, 4259 (1976).
[29] J. R. Franz, P. Brauers and C. Holzhey, J. Phys. F **10**, 235 (1980).

$$H = \sum_n \epsilon_n |n><n| + \sum_{n \neq m} t_{nm} |n><m|$$

where $|n>$ is a localized state at site n and t_{nm} are hopping integrals between first neighbour sites. The site energy level ϵ_n for an A-type atom, say, is taken to depend on the amount of charge gained or lost by the atom for a given value of the concentration, as well as on a short-range order parameter measuring the average occupation of neighbouring sites by B-type atoms relative to a random alloy. A calculation of single particle Green's functions yields the on-site densities of states, from which the charge transfer can be evaluated up to self consistency. The short-range order parameter is finally determined by minimizing the free energy.

A charge transfer of about 0.6 electrons from Cs to Au is found for Cs-CsAu over the whole range of composition, combined with an excess probability for unlike neighbours with a maximum at equimolar composition. Such an increase of local order of the two species with gold concentration from the pure Cs end counterbalances the increasing width of the Au band of states, yielding a pseudogap at all compositions in this range. The broadening of the Au band finally destroys the gap on further addition of gold beyond equimolar composition. The behaviour of the density of states with composition is shown in Figure 18.a (the lower band contains predominantly gold states and the upper one cesium states), and Figure 18.b shows the calculated density of states at the Fermi level as a function of composition. With these results, satisfactory contact can be made with data on electric conductivity, magnetic susceptibility, and Knight shifts.

Considering next the whole series of alkali-gold alloys at equimolar composition, transport measurements indicate that the transition from metallic to nonmetallic behaviour occurs between NaAu and RbAu, with KAu near the borderline. From the tight binding model of Franz et al, the density of states at the Fermi level and the gap can be represented through the series of systems as functions of the ratio $\Delta\phi/<t>$ between the electronegativity difference and an average hopping integral (see Figure 19[30]). Since the average hopping integral varies through the series in parallel with the electron density (increasing from CsAu to LiAu), the nonmetal-metal transition can be viewed in essence as a Mott transition occuring when the electronic screening length becomes comparable with the distance between unlike ions. Screening is most effective in LiAu, where the electron density is highest, whereas at the other extreme it cannot prevent Coulomb interactions from opening the gap in CsAu.

[30] C. Holzhey, F. Brouers, J. R. Franz and W. Schirmacher, J. Phys. F 12, 2601 (1982).

5.3 Other alkali-based alloys with chemical short range order. Interspecies ordering has also been reported for a number of other alkali-based alloys, the alloying partners being elements of group III, IV and V (see e.g. Meijer et al[31]). The formation of chemical order at certain compositions is signalled by anomalies in electronic properties such as the electrical resistivity and the magnetic susceptibility, which reflect a minimum in the density of states at the Fermi level if not the opening of a gap due to full charge transfer. An illustration of resistivity behaviours in alloys with group IV elements is given in Figure 20. Three different kinds of compound formation are represented:

(i) compound formation near the octet composition A_4B, as in Li-Pb and Li-Sn;

(ii) compound formation near the equimolar composition AB, as in K-Pb and Rb-Pb;

(iii) compound formation near both the above compositions, as in Li-Si, Li-Ge and Na-Sn.

The available data indicate increasing stability of the octet composition compound through the sequence Si, Ge, Sn and Pb, and decreasing stability through the series from Li to Cs.

We have already seen in Figure 8 a direct observation by neutron diffraction of the chemical order in liquid Li_4Pb.[5] The dynamics of concentration fluctuations in this liquid has also been studied by neutron quasi-elastic scattering.[32] A qualitative picture of the electronic density of states in this system involves a valence band derived from the outer p states of Pb, which is filled by electrons from the 2s band of Li in a process in which charge transfer and local chemical order are mutually reinforcing each other. A local minimum in the density of states at the Fermi level, rather than a pseudogap between the valence and the conduction band, is expected from the fact that Li_4Pb is still metallic, though with a rather high resistivity (see Figure 20).

For the alloys in the classes (ii) and (iii), instead, Meijer et al[31] have proposed a model for order at equimolar composition which invokes formation of essentially tetrahedral Pb_4^{4-} or Sn_4^{4-} polyanions, such tetrahedra being seen in the solid structure of the equiatomic compound. In such a tetrahedral cluster the p states of Pb, say, would be split into bonding and antibonding states and the former could be filled by electrons from the alkali atoms.

5.4 Tellurium-based alloys. Formation of chemical short range order has also been studied in liquid alloys formed by Te with metals such as Ni, Cu, Ag and Tl. Pure Te in the solid phase is a semiconductor with a structure consisting of helical chains, which is believed to change on melting into a 3D network of covalent bonds. Some of the valence electrons are still localized in the bonds, while the rest form a sea of conduction electrons. Notable behaviours of the electric resistivity of liquid Te-based alloys are[21] a sharp minimum in the conductivity at "stoichiometric" compositions corresponding to

[31] J. A. Meijer, W. Geertsma and W. van der Lugt, J. Phys. F 15, 899 (1985).
[32] M. Soltwisch, D. Quitmann, H. Ruppersberg and J. B. Suck, Phys. Rev. B 28, 5583 (1983).

Ag_2Te, Cu_2Te and Tl_2Te, whereas in Ni-Te a continuous increase in conductivity is observed up to a composition corresponding to Ni_2Te.

The observed electronic transport properties have been related to the observed liquid structure in both Ni-Te and Cu-Te, an important role being played by d electrons. Figure 21 shows the measured radial distribution functions in Ni-Te at two compositions.[33] These give clear evidence of chemical short range order combined with a strong penetration of Ni atoms into the first coordination shell of a Ni atom, the Ni-Ni coordination number being of order 2-3 against a Ni-Te coordination number of order 4-5. It is also remarkable that the Te-Te coordination number is increased from about 3 in pure liquid Te to about 10 in the two alloys, and that the Te-Te distance is similarly increased from 2.91 Å to about 3.55Å. The Te atoms in the alloys form an essentially close packed structure similar to that of chlorine ions in molten alkali chlorides: this suggests that Ni and Te are behaving as cations and anions, respectively, while at the same time the close contact between Ni ions gives appreciable overlap between their d states to yield metallic d bonds.

The liquid structure of CuTe is broadly similar to that of NiTe, but the resistivity increases on alloying in the former system and decreases in the latter. The difference in electronic behaviours has been related[34] to differences in d electron structure and to the location of the Fermi level relative to the d bands in the two systems. Considering here only the Cu_2Te stoichiometric composition, it is evident that the presence of Cu^+ ions in the d^{10} configuration will naturally lead to a low conductivity.

[33] V. T. Nguyen, M. Gay, J. E. Enderby, R. J. Newport and R. A. Howe, J. Phys. C 15, 4627 (1982).
[34] R. J. Newport, R. A. Howe and J. E. Enderby, J. Phys. C 15, 4635 (1982).

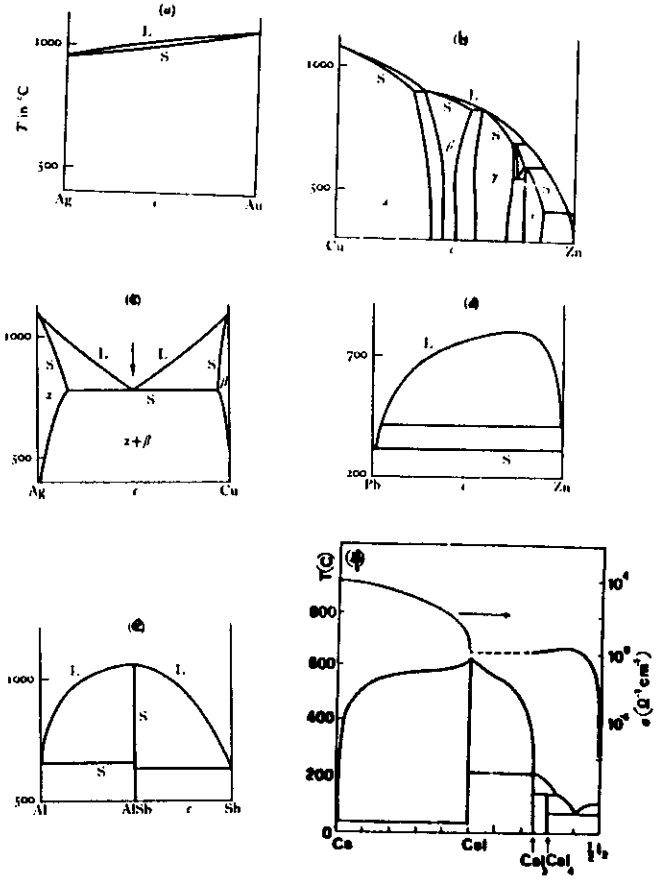

Figure 1. Typical phase diagrams for binary alloys. Diagram (f), for the Cs - I system, shows also the electrical conductivity of the liquid (upper curve, with scale on the right).
S = solidus, L = liquidus.

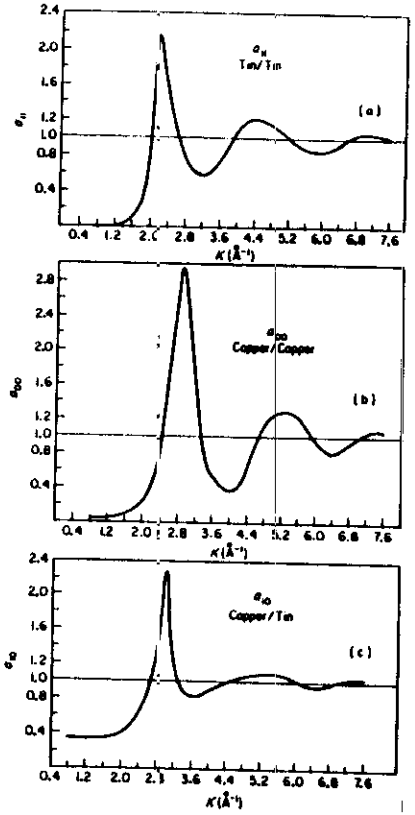

Figure 2. Partial structure factors in liquid Cu_6Sn_5 system, as obtained by neutron scattering through isotopic substitution (from Enderby, North and Egelstaff, 1966)

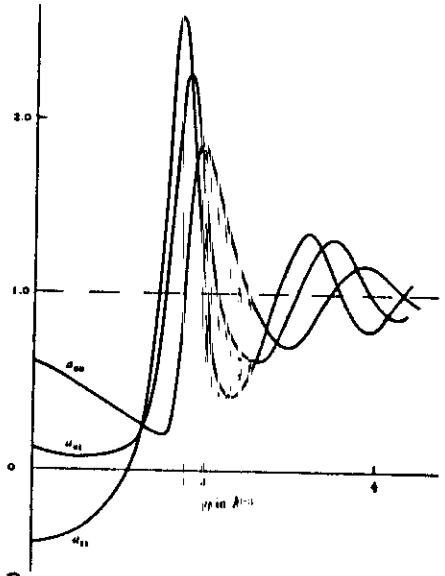

Fig. 3. Partial interference functions according to the Percus–Yevick rigid-sphere model for $c_1 = \frac{1}{4}$, $y = 0.48\pi$, $\ldots = 1.24$. (After Enderby & North, 1968.)

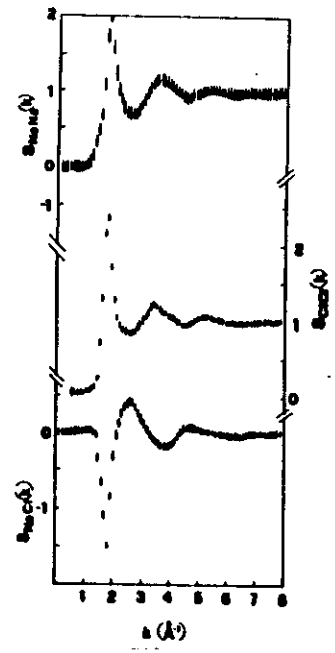

Figure 4. The partial structure factors of molten NaCl at 875°C (from Biggin and Enderby 1982).

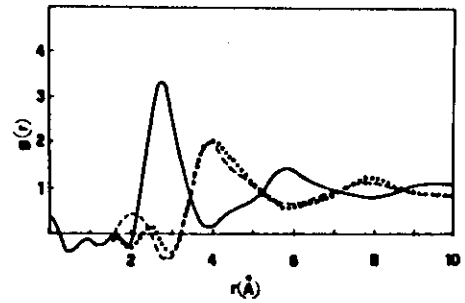

Figure 5. The pair distribution functions of molten NaCl at 875°C: full curve, g_{NaCl}; dotted curve, g_{ClCl}; broken curve, g_{NaNa}. From Biggin and Enderby (1982).

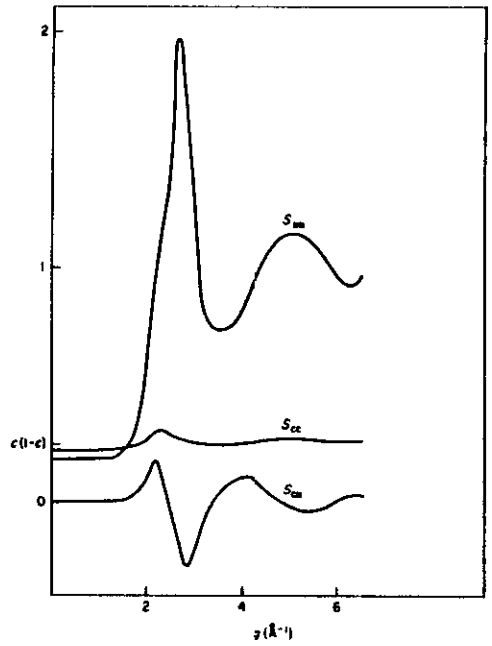

Figure 6 Number - concentration structure factors for the copper-tin alloy of *figure 5* (from Bhatia and Thornton, 1970)

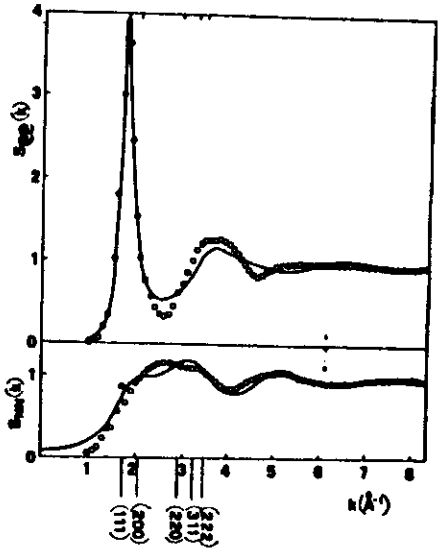

Figure 7. The Bhatia-Thornton structure factors $S_{cc}(k)$ and $S_{NN}(k)$ of molten NaCl near freezing, from neutron diffraction data (circles) and from HNNC theory of a pair potentials model (curves). The location of the first few stars of reciprocal lattice vectors of the NaCl-type structure, after adjustment of the (111) star to the peak of $S_{NN}(k)$, is shown on the horizontal axis.

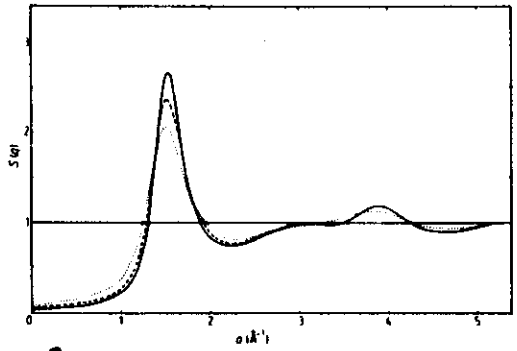

Figure 8 Total structure factors $S(q) = S_{xx}(q)c_x^2$ of liquid Li_xPb measured by neutron diffraction at 995 K (full curve), 1075 K (broken curve) and 1225 K (dotted curve)

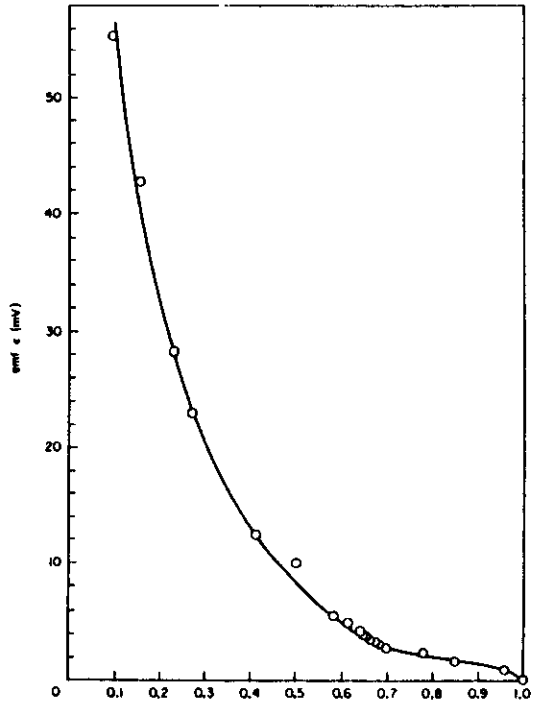

Figure 9 Emf (in mV) of the liquid Na–Cs alloy as a function of Na concentration. The points are experimental data of Ichikawa and Thompson (1974) and the curve is based on Flory's model, including size effects and interchange energy (from Bhatia and March, 1975)

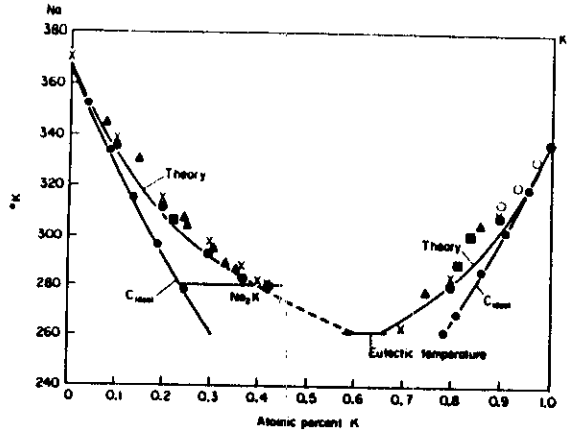

Figure 10. Liquidus curve in Na–K alloys (from Bhatia and March, 1972)

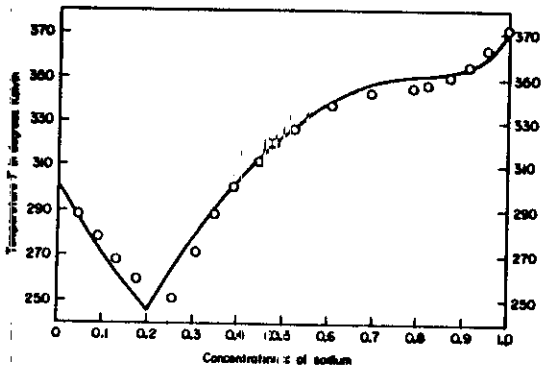

Figure 11. Liquidus curve of the Na–Cs system against Na concentration: symbols are as in *figure 8* (from Bhatia and March, 1975)

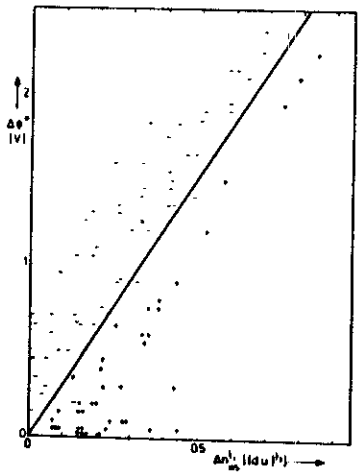

Fig. 12. Demonstration of the reliability of eq. (7) in predicting the sign of the heat of mixing of liquid alloys not containing transition or noble metals. Each symbol corresponds to one binary system. The meanings of the signs are: ○: ΔH^{mix} < − 2.5 kJ/mole of atoms of the equiatomic composition; +: ΔH^{mix} > +2.5 kJ/mole of atoms of the equiatomic composition, or the liquid system has a central miscibility gap, or the solubility of at least one of the metals is very small at temperatures above 1000 K.

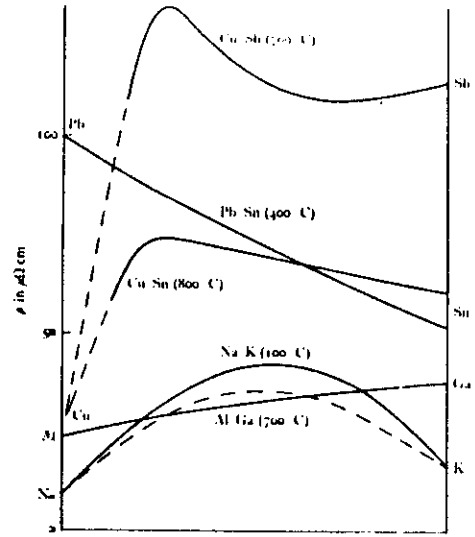

Fig. 13. Experimental resistivity isotherms for some typical liquid alloys. The broken curve for Na–K is a theoretical one due to Ashcroft & Langreth (1967*b*).

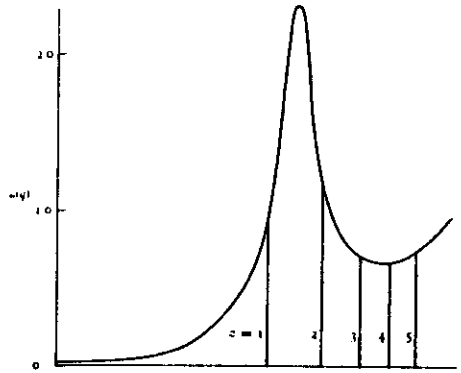

Fig. 14. Vertical lines mark the limit of integration in Ziman's formula corresponding to $q = 2k_F$. Its position relative to the main peak in $a(q)$ depends on the valency of the metal.

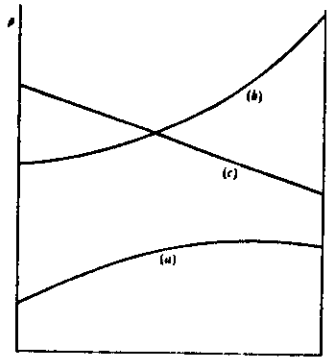

Fig. 15. Resistivity isotherms to be expected for mixtures of (*a*) two monovalent metals, (*b*) two divalent metals, (*c*) two polyvalent metals in the liquid state.

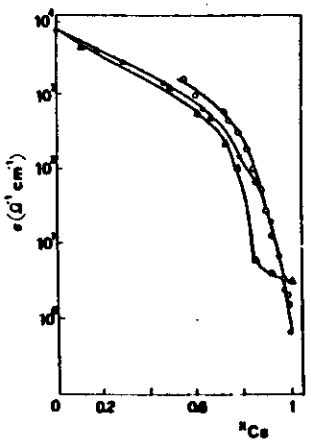

Figure 16. Electrical conductivity vs concentration for Cs-CsAu (triangles), Cs-CsI (dots) and Cs-CsCl (circles) at 650°C. From Sotier et al (1984).

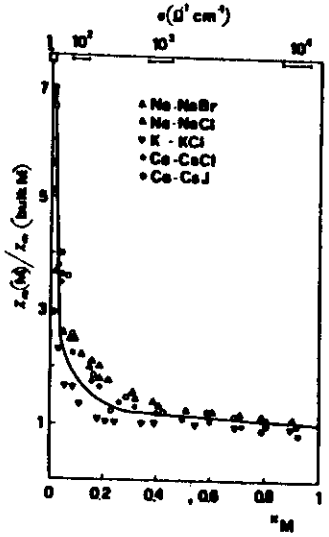

Figure 17. Excess magnetic susceptibility of metal-molten salt solutions at 1100°C, in units of the Pauli susceptibility of the metal, as a function of metal concentration x_M. The empty square on the vertical axis shows the Curie susceptibility of an isolated spin, while the bars near the top of the figure give ranges of concentration in which the electrical conductivity of the solutions has the indicated values. From Nicolosc and Freyland (1983b).

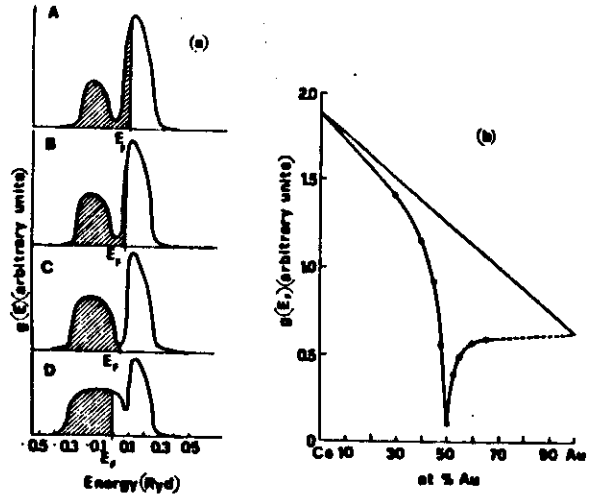

Figure 18. Calculated density of electron states g(E) in liquid Cs-Au at 600°C (from Franz et al 1980). (a) g(E) vs energy at 30 (A), 40 (B) 50 (C) and 60 (D) at % Au. The shaded areas indicate the occupied states. (b) g(E) at the Fermi energy E_F as a function of concentration. The straight line is the linear interpolation between the values calculated for the pure liquids.

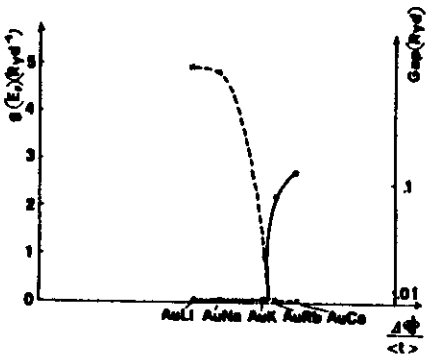

Figure 19. Density of states at the Fermi energy (crosses joined by broken curve) and width of the gap (dots joined by full curve) for stoichiometric alkali-gold alloys, as functions of the ratio $\Delta\phi/\langle t\rangle$. From Holsey et al (1982).

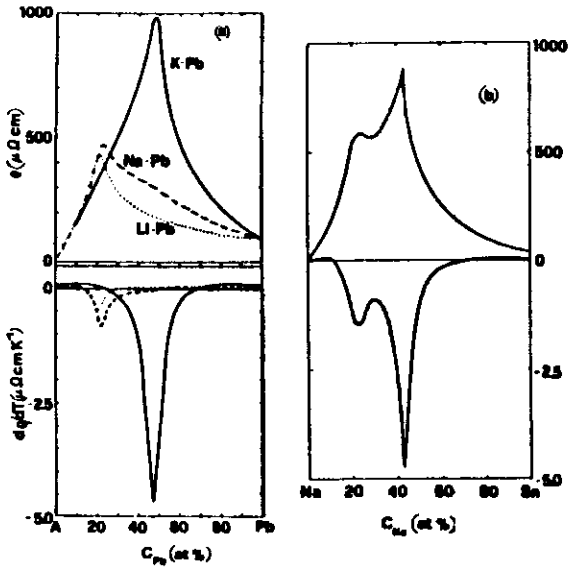

Figure 20. Electrical resistivity ρ (top) and its temperature derivative (bottom) for liquid alkali-Pb systems (a, from Meijer et al 1985) and for Na-Sn (b, from van der Lugt and Geertsma 1984).

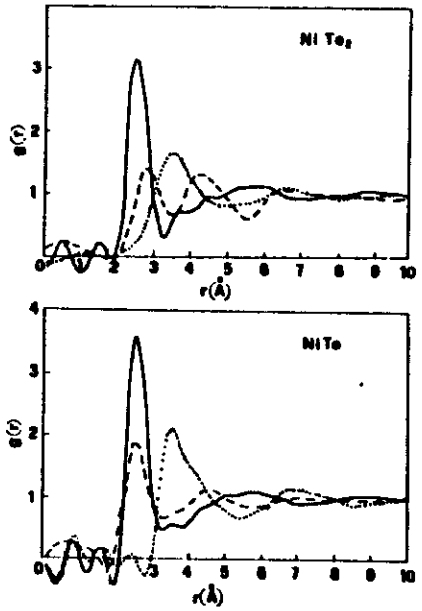

Figure 21. Partial pair distribution functions in liquid $NiTe_2$ and NiTe at 930C: full curves, g_{NiTe}; broken curves, g_{NiNi}; dotted curves, g_{TeTe}. From Nguyen et al (1982).